MHD PROCESSES IN THE CHANNEL OF A FLAT INDUCTION PUMP WITH BARRIERS

A. F. Boyarintsev, L. M. Dronnik
S. Yu. Reutskii, and I. M. Tolmach

UDC 538.4:621.313.333

The steady-state motion of a liquid metal with electrical conductivity σ in a fixed-width channel of a flat induction pump under the action of a magnetic field traveling along the x axis is studied (Fig. 1). The transverse cross section of the channel is divided by longitudinal conducting barriers (their number is fixed and finite) with conductivity σ_1 into a series of hydraulically identical parallel subchannels. The thickness of the barrier equals Δ, the thickness of the walls equals Δ_1, the total width of the channel equals 2α (neglecting the barriers), and the pole interval equals τ. The barriers are usually inserted into the channels of large induction rectilinear pumps in order to prevent overflows and to provide strength.

In this work we performed a combined analysis of the influence of the transverse edge effect and hydrodynamic effects using the model of narrow flow strips in the presence of a finite number of barriers in the channel, taking into account the sticking of the flow to the walls of the barriers.

The new feature, compared with [1], is the fact that the effect of the finite number of conducting barriers is taken into account.

Neglecting the convective terms, we write the equation of motion for the average quantities in the form [1]

$$-\frac{d}{dy}\left[(\eta_T+\eta_L)\frac{du}{dy}\right]-\frac{\lambda_m}{8\delta}\rho u|u|-\frac{\alpha}{2\mu_0}B_m\,\mathrm{Im}(\dot{b}(y))-\frac{\partial p}{\partial x}=0. \quad (1)$$

Here η_L is the dynamic viscosity while η_T is the turbulent viscosity; λ_m is the drag; $\dot{b}(y)$ is the complex amplitude of the induced field; B_m is the amplitude of the external field; and, $\partial p/\partial x$ is the pressure gradient. Like in [1], the problem is studied in the approximation of a plane-parallel field with only a z component. In this case the induction equation has the form

$$d^2\dot{b}/d\bar{y}^2=\dot{b}+i\,\mathrm{Rm}\,(1-u)\,(1+\dot{b}), \quad (2)$$

while the components of the current density $\dot{j}_x = \partial\dot{b}/\partial y$, $\dot{j}_y = i\dot{b}$. The overbars denote dimensionless quantities, introduced by the relations (in what follows the overdot for $\bar{b}$ is omitted for simplicity):

$$\bar{y}=\alpha y,\ \bar{b}=b/B_m,\ \ \bar{u}=u/v_s=u\alpha/\omega, \quad (3)$$

while $\mathrm{Rm} = \sigma\mu_0\omega/\alpha^2$ is the magnetic Reynolds number.

In the barriers and walls of the channel, instead of (2) we have

$$d^2\bar{b}/d\bar{y}^2=\bar{b}+i\,\mathrm{Rm}_1\,(1+\bar{b}),\ \ \mathrm{Rm}_1=(\sigma_1/\sigma)\,\mathrm{Rm}. \quad (4)$$

We use two expressions for the turbulent viscosity η_T: first,

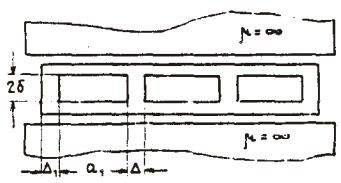

Fig. 1. Diagram of the flow.

Translated from Magnitnaya Gidrodinamika, No. 3, pp. 111-114, July-September, 1987. Original article submitted November 12, 1986; revision submitted December 19, 1986.

 0024-998X/87/2303-0326$12.50

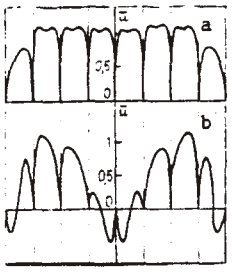

Fig. 2

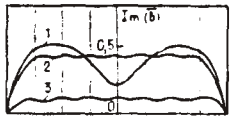

Fig. 3

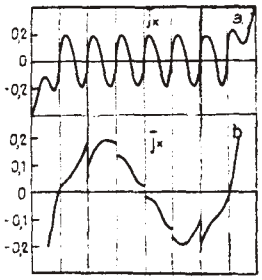

Fig. 4

Fig. 2. Velocity profile for s = 0 (a) and s = 0.8 (b).

Fig. 3. Electromagnetic force density distribution. s = 0.8 (1), 0.2 (2), and 0 (3).

Fig. 4. The $\bar{j}_x$ component of the induced current density for s = 0 (a) and 0.8 (b).

$$\eta_T = \text{const}, \tag{5a}$$

as in [1], and, second,

$$\eta_T = \rho l^2 \left| d\bar{u}/dy \right|, \tag{5b}$$

where $l = 0.4y_w$ is the Prandtl mixing length [2], y_w is the distance to the nearest solid wall. Using (3) we write the equation of motion (1) in the dimensionless form

$$\frac{d}{d\bar{y}}\left\{\left(1+\mathrm{Re}\,l^2\left|\frac{d\bar{u}}{d\bar{y}}\right|\right)\frac{d\bar{u}}{d\bar{y}}\right\} - q\bar{u}|\bar{u}| - \frac{1}{2}\frac{\mathrm{Ha}^2}{\mathrm{Re}}\,\mathrm{Im}\,(\delta(y)) - \varkappa = 0. \tag{6}$$

Here $\mathrm{Re} = \rho v_s/\eta\alpha$ is the Reynolds number; $\mathrm{Ha} = (B_m/\alpha)\sqrt{\sigma/(\rho\nu)}$ is Hartmann's number; $q = \lambda_m \rho v_s/(8\delta\eta\alpha^2)$, $\varkappa = (\partial p/\partial x)/(\eta v_s \alpha^2)$.

At the solid boundaries we have u = 0. For the magnetic field $\bar{b}$ at each interface the conditions

$$\bar{b}_k = \bar{b}_{k+1},\ \sigma_k^{-1}(d\bar{b}_k/dy) = \sigma_{k+1}^{-1}(d\bar{b}_{k+1}/d\bar{y}) \tag{7}$$

hold.

On the exterior, air side of the lateral wall of the channel, $\bar{b} = 0$.

The system of equations (2), (4), and (6) was solved by the method of finite differences (the algorithm is described in [1]). If (5b) is employed for η_T, then it is refined iteratively. We present below some results of the solutions.

Figure 2 shows the profile of the velocity in the transverse section of the channel; Figure 3 shows the electromagnetic force density; and, Fig. 4 shows the distribution of the component j_x of the induced current density. The calculations show that as the slipping varies from the 0 to 0.4 the flow rate in each of the eight subchannels of the pump decreases monotonically; at the same time, on the whole the form of the velocity profile corresponding to s = 0 is preserved. Dips at the center of each subchannel can be distinguished in the velocity profile in this range of slippings, while the electromagnetic force profile has a wavy character. This is explained by the appearance of an eddy of induced current, which is closed along the barriers (see Fig. 4a), in each of the subchannels. The breaks in Fig. 4 are explained by the fact that the distribution of the current density in the barriers, whose thickness is much less than the width of the subchannel, is not shown. As the slipping is increased further (s > 0.4) the distribution of the current, electromagnetic force density, and velocity changes significantly. Separate current vortices, closing within one subchannel, vanish. A general vortex of the current density, closed on the total width of the channel, appears (Fig. 4b). This is also reflected in the distribution of the electromagnetic force. Owing to the demagnetizing effect of the current density vortex it is distributed nonuniformly (in an M-shaped manner) in the transverse section (curve 1 in Fig. 3). The velocity profile also becomes redistributed correspondingly, and in the central subchannels we have $\bar{u} < 0$ (Fig. 2b).

The change in the character of the velocity, current, and field distributions in the transverse section also affects the integral characteristics of the pump. Figure 5 shows

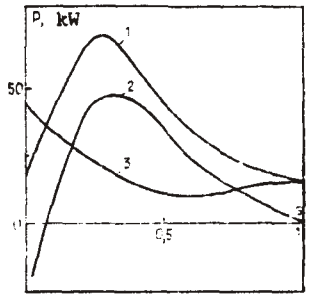

Fig. 5

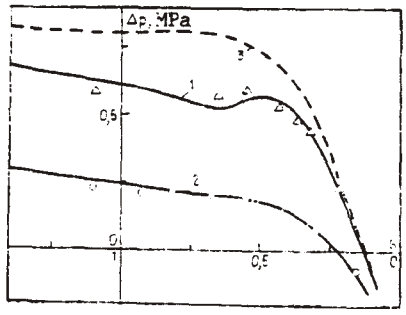

Fig. 6

Fig. 5. Energy characteristics: 1) electromagnetic power, 2) hydraulic power, 3) friction power loss.

Fig. 6. External characteristics of AMN-6. B_m: 0.32 (1), 0.205 T (2); curve 3 shows the calculation neglecting the distribution of $\bar{u}$ (see explanation in the text).

a graph of $P_{e\ell}$, P_{hyd}, P_{fr} as a function of the average slipping. The change in the friction losses P_{fr} should be noted: as the slipping increases from 0 to ≈0.5 it decreases monotonically, similarly to the manner in which this would happen in the case of the motion of a solid. But, taking into account the nonuniformity of the velocity profile distribution over the width of the channel, P_{fr} equals

$$P_{fr} = \int_0^{2a} \left[\left(1 + \mathrm{Re}\,\bar{\gamma}^2 \left| \frac{d\bar{u}}{d\bar{y}} \right| \right) \left(\frac{d\bar{u}}{d\bar{y}} \right)^2 + q|\bar{u}|\bar{u}^2 \right] d\bar{y}.$$

As the slipping increases further ($s \gtrsim 0.5 \ldots 0.6$) P_{fr} ceases to decrease and even increases somewhat, which is explained by the intense mixing of metal in the states close to the locked channel (see also Fig. 2b).

Figure 6 compares the calculation of p(Q) characteristic of the AMN-6 pump with the experiment described in [3]. We give below a generalized expression for the electromechanical power, taking into account approximately the transverse, longitudinal, and depth edge effects, the effect of the barriers and the nonuniform distribution of the velocity in the transverse section of the channel [1]:

$$P_{el} = {}^1/_2 \sigma v_{av}^2 B_m w \{-s/(1-s) k_s k_{ps} k_l + C_0 - C_l - C_r\}. \quad (8)$$

The coefficients k_s, k_{ps}, k_ℓ, C_0, C_ℓ, C_n are determined from the solutions of separate boundary-value problems, which are not studied here. The formula (8) makes it possible to calculate, for fixed slipping, induction amplitude, and temperature, the electromechanical power injected into the liquid metal.

At the same time the solution of the problem formulated above permits calculating the friction losses, corresponding to the nonuniform profile of the velocity in the transverse cross section of the channel. This, in its turn, makes it possible to find the working pressure drop in the pump using the formula

$$\Delta p = (P_{el} - P_{fr})/Q. \quad (9)$$

For comparison the broken line for $B_m = 0.32$ T shows the p(Q) characteristic also calculated using the formulas (8) and (9), but for friction losses equal to ξQ^3, where ξ is the generalized drag, determined from flow tests. In this case the computed and experimental data agree only for small slippings ($s \lesssim 0.4$). At the same time taking into account the friction based on the nonuniform profile gives good agreement with experiment over the entire range of slippings.

Let us examine the effect of the conductivity of the barriers on the energy characteristics of the pumps. Two cases were analyzed: 1) channel with nonconducting barriers ($Rm_1 = 0$) and 2) channel with conducting barriers. The calculations were performed for a pump with the following parameters: $\tau = 0.225$ m, $2a = 1$ m, $\Delta = \Delta_1 = 0.004$ m, $\delta = 0.02$ m, $\sigma = 5.35 \cdot 10^6$ S/m, $\sigma_1 = 0.95 \cdot 10^6$ S/m, $\rho = 868$ kg/m^3, L_A is the length of the working section of the channel equal to 3.8 m; $B_m = 0.3$ T.

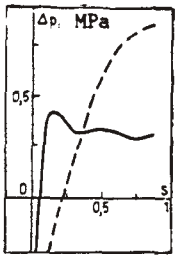

Fig. 7

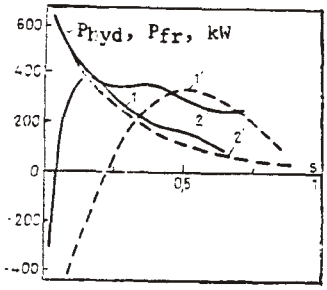

Fig. 8

Fig. 7. Effect of the finite conductivity of the barriers.

Fig. 8. Hydraulic power (1, 1') and friction losses (2, 2').

Figure 7 shows a graph of the pressure drop Δp versus the slipping s. The broken curve was constructed for a pump with nonconducting barriers, the solid line is for $\sigma_1 = 0.95 \cdot 10^6$ S/m.

Figure 8 shows, for the same conditions, graphs of the hydraulic power (curves 1, 1') and friction losses (2, 2'). For small slippings there are virtually no friction losses in both cases; then in the case of a channel with nonconducting barriers they continue to decrease monotonically, while in a channel with conducting barriers the curve of P_{fr} versus the slipping has a wavy character and decreases much more slowly. This is attributable to the fact that in a channel with conducting barriers the flow becomes unstable because of the nonuniform distribution of the electromagnetic force. The nonconducting barriers break the electrical coupling between the subchannels, prevent the development of instability, and reduce the friction losses because of the more uniform flow. At the same time the presence of nonconducting barriers increases the Joule losses in the channel. Therefore in order to choose one variant over the other it is necessary to analyze in detail all processes occurring in the channel pump.

LITERATURE CITED

1. B. B. Volchek, L. M. Dronnik. S. Yu. Reutskii, and I. M. Tolmach, "Transverse edge effect in flat induction pumps with input," Magn. Gidrodin., No. 4, 93-100 (1981).
2. G. Shlichting, Boundary Layer Theory, McGraw-Hill (1968).
3. I. M. Tolmach, E. Z. Asnovich, P. G. Goloborod'ko, L. M. Dronnik, Ya. Ya. Zandart, A. I. Klimenko, I. A. Liepin'sh, S. Yu. Reutskii, and V. E. Strizhak, "Experimental study of a two-module assembly of flat induction pumps," in: 11th Riga Conference on Magnetohydrodynamics, Vol. 2, Institute of Physics of the Latvian SSR Academy of Sciences, Salaspils (1984), pp. 23-26.